

---

# **Oxide Based Particulate Filters for Light-Duty Diesel Applications – Impact of the Filter Length on the Regeneration and Pressure Drop Behavior**

**Thorsten Boger and Ingo-C. Tilgner**  
Corning GmbH

**Min Shen and Yi Jiang**  
Corning Incorporated

Reprinted From: **Diesel Exhaust Emission Control, 2008**  
(SP-2154)

ISBN 978-0-7680-1635-2



**SAE** *International*<sup>™</sup>

**2008 World Congress**  
**Detroit, Michigan**  
**April 14-17, 2008**

By mandate of the Engineering Meetings Board, this paper has been approved for SAE publication upon completion of a peer review process by a minimum of three (3) industry experts under the supervision of the session organizer.

All rights reserved. No part of this publication may be reproduced, stored in a retrieval system, or transmitted, in any form or by any means, electronic, mechanical, photocopying, recording, or otherwise, without the prior written permission of SAE.

For permission and licensing requests contact:

SAE Permissions  
400 Commonwealth Drive  
Warrendale, PA 15096-0001-USA  
Email: [permissions@sae.org](mailto:permissions@sae.org)  
Tel: 724-772-4028  
Fax: 724-776-3036



For multiple print copies contact:

SAE Customer Service  
Tel: 877-606-7323 (inside USA and Canada)  
Tel: 724-776-4970 (outside USA)  
Fax: 724-776-0790  
Email: [CustomerService@sae.org](mailto:CustomerService@sae.org)

**ISSN 0148-7191**

**Copyright © 2008 SAE International**

Positions and opinions advanced in this paper are those of the author(s) and not necessarily those of SAE. The author is solely responsible for the content of the paper. A process is available by which discussions will be printed with the paper if it is published in SAE Transactions.

Persons wishing to submit papers to be considered for presentation or publication by SAE should send the manuscript or a 300 word abstract of a proposed manuscript to: Secretary, Engineering Meetings Board, SAE.

**Printed in USA**

# Oxide Based Particulate Filters for Light-Duty Diesel Applications – Impact of the Filter Length on the Regeneration and Pressure Drop Behavior

Thorsten Boger and Ingo-C. Tilgner  
Corning GmbH

Min Shen and Yi Jiang  
Corning Incorporated

Copyright © 2008 SAE International

## ABSTRACT

Diesel particulate filters are becoming a standard for most light duty diesel applications designed for European EU5 and EU6 regulations. Oxide based filter materials are continuing to gain significant interest and have been in high volume serial application since 2005. Compared to carbide materials they show some unique properties.

With respect to the design, the length of a filter is a key variable. Usually the prime design consideration is the desired filter volume. The diameter or frontal area is then usually defined by packaging constraints. Finally, the length is adapted. The paper provides experimental data on the impact this key design parameter has on the pressure drop and the thermal behavior under “worst case” regeneration conditions. A wide range of soot loads (from 4 g/dm<sup>3</sup> to 9 g/dm<sup>3</sup>) as well as filter lengths from 6” to 12” is considered and evaluated under comparable experimental conditions.

The discussion is based on experimental data as well as numerical simulations with a 2D simulator. The simulator is shown to be in good agreement with the experimental observations. In general shorter filters are found to be of advantage. They provide for lower pressure drop and yield lower temperatures and gradients during worst case regeneration conditions. Data are provided that can help to estimate the impact of the filter length on the soot mass limit.

## INTRODUCTION

The application of particulate filters to European passenger cars with diesel engines continues to be growing at a fast rate. For EU5 it is expected that most diesel engines will have to be equipped with a diesel particulate filter to meet the further reduced particulate matter emission standards. After the initial introduction of SiC based filters, oxide based particulate filters are gaining significant interest [1-3]. More than 750,000 aluminum titanate filters (Corning DuraTrap<sup>®</sup> AT) will be

on the road by the end of 2007. Cordierite filters are today in series production on most heavy and a large number of medium duty applications to meet US 07 regulations [4, 5]. For the near future a number of passenger car series applications are expected as well. Although comparable from a filtration perspective [3] the oxide filters show different thermal behavior compared to SiC, especially due to the difference in thermal conductivity. The lower thermal conductivity of oxide materials generally allows for a faster heat up and regeneration but also requires some adaptation with respect to the optimal regeneration strategy [6].

Across the applications there is a clear trend towards close-coupled installations of the particulate filter. However, in some instances space constraints in the engine compartment prevent such installation. In the underfloor position usually it is easier to allocate space for the aftertreatment components. However, other than operational difficulties with heat losses etc., the underfloor installations are commonly constrained in the available frontal area and height of the filter to maintain a sufficient chassis clearance. Therefore the filter length is used to adjust the filter to the desired volume allowing for sufficient soot and ash storage capacity.

It is common understanding that the soot mass limit of a particulate filter decreases with increasing filter length [8,9]. However, very little quantitative information is available on the impact of this important design parameter especially for oxide filter materials. The objective of this paper is to address this question and provide experimental confirmation as well as a thorough fundamental understanding.

## EXPERIMENTAL SETUP AND PROCEDURES

The experimental work was performed with a two liter prototype engine designed to meet EU4 standards. The engine had common rail fuel injection system, turbo charger, intercooler, and cooled exhaust gas recirculation (EGR). The engine was installed in a dynamic test bench with an

asynchronous dynamometer. The test bench was equipped with an emission bench for transient exhaust gas analysis, an AVL 415S smoke meter and a constant volume sampling (CVS) system for dedicated experiments. In addition to the engine sensor readings and the data from engine control unit (ECU), the test bed had standard instrumentation with several additional temperature and pressure sensors, mass flow controller, etc.

The aftertreatment system comprised an oxidation catalyst (400 cps) followed by the catalyzed diesel particulate filter (see Fig. 1). For the testing program, a series of cordierite filters (Corning DuraTrap® AC 300/15 ACT) with a nominal cell density of 300 cps and 15 mil wall thickness were used. The coating on the particulate filter had a relatively low precious metal content, which was mainly designed to convert the CO generated during the soot oxidation. Filters with different lengths of 6", 8", 10" and 12" were used in the program. All had the same diameter and same nominal catalyst coating. Filter data are summarized in Table 1.

**Table 1.** Dimensions of filters used. All were Advanced Cordierite filters with nominal cell density/wall thickness of 300/15 and asymmetric cell technology (ACT).

Filter	A	B	C	D
<b>Length</b>	6 inch 152.4 mm	8 inch 203.2 mm	10 inch 254.0 mm	12 inch 304.8 mm
<b>Diameter</b>	5.2 inch 132.1 mm			
<b>Volume</b>	2.09 dm <sup>3</sup>	2.78 dm <sup>3</sup>	3.48 dm <sup>3</sup>	4.18 dm <sup>3</sup>

To record the thermal events during severe regeneration experiments all filters were equipped with 28 thermocouples. Schematics of the thermocouple patterns used for the filters with different lengths are shown in Figure 2. In all cases the main focus was to capture the temperatures in the rear of the tested filter.

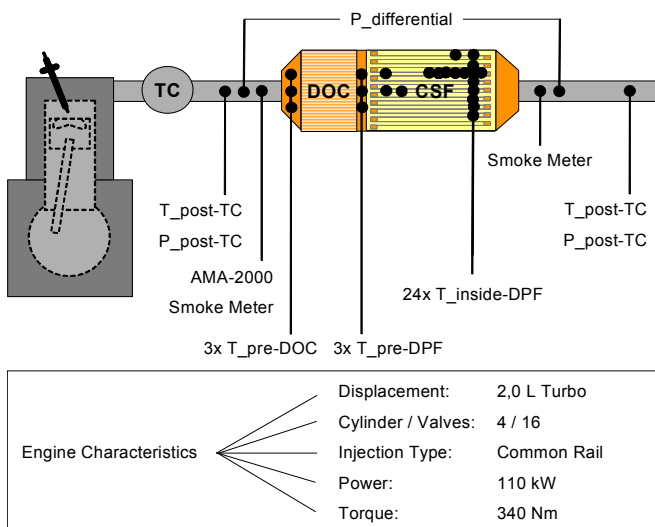


**Figure 1.** Schematic of the test setup.

Due to imperfections in the radial temperature distribution at the filter inlet, 3 additional thermocouples in different radial positions have been installed just at upstream of both the diesel oxidation catalyst (DOC) and the filter.

For the tests, the filters were canned by a simple stuffing method. To stabilize the weight of the canned filters, especially with respect to the mat, the canned filters were heat-treated in a furnace for several hours.

Different experiments were performed on engine bench. Prior to all tests the filters have been conditioned by several hours of operation of the filter on engine bench at full load and speed. The soot loading was done at a steady state engine operating point with a relatively high soot loading rate of 5-6 g/h. The soot mass accumulated on the filter was monitored through weighing and adjusted to within +/- 0.5 g/dm<sup>3</sup> of the target soot load. Experiments at different specific soot loads up to 9 g/dm<sup>3</sup> were included.

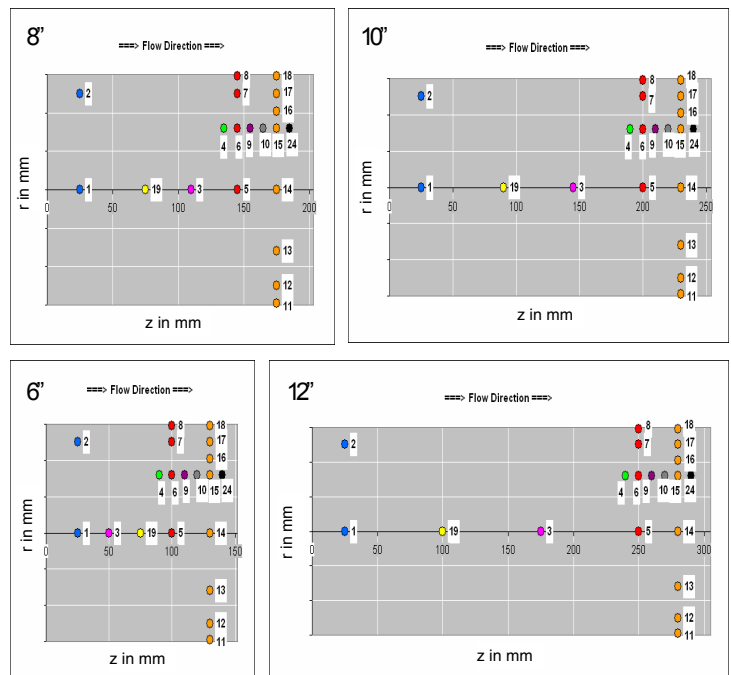


**Figure 2.** Thermocouple patterns used within the filters of different lengths. Shown is the 0°-180° plane.

A dynamic test procedure was used for the pressure drop experiments. This procedure consists of a short conditioning phase, where the filter is stabilized at ~250 °C followed by a rapid increase in engine speed and load (up to the maximum fueling rate). Then the fueling is decreased to zero within a short timeframe, e.g. the torque is reduced to zero while the speed is maintained. The entire procedure takes only a few minutes and has been found to deliver reliable results. Due to the short duration the temperature at the filter inlet stays relatively constant at ~350-400 °C throughout the relevant test phase.

The regeneration experiments were limited to severe drop to idle tests (DTI experiments). In these experiments an active regeneration is initiated at a low load, medium speed engine operating condition. After a fixed time, when the filter inlet temperature reached 600 °C, the engine is switched back to idle. This results in a sudden increase in the oxygen concentration of the exhaust gas and a significant decrease in mass flow. An example of the conditions during such a DTI test is shown in Figure 3. This test has been found to represent some of the worst case conditions as the soot has started to burn, sufficient oxidant (O<sub>2</sub>) is provided and the convective heat removal is drastically reduced. The rate at which the heat is released exceeds the heat that can be removed from the system, leading to an increase in the temperature inside the filter, resulting in thermomechanical stress. After each regeneration experiments the soot mass burned was determined gravimetrically. Then the residual soot was burned in a clean out regeneration step at constant engine operating conditions. At the end of the clean out step another weight measurement was used to check that all soot had been burned. Prior to the next regeneration experiment, the filter was reloaded to the desired soot level.

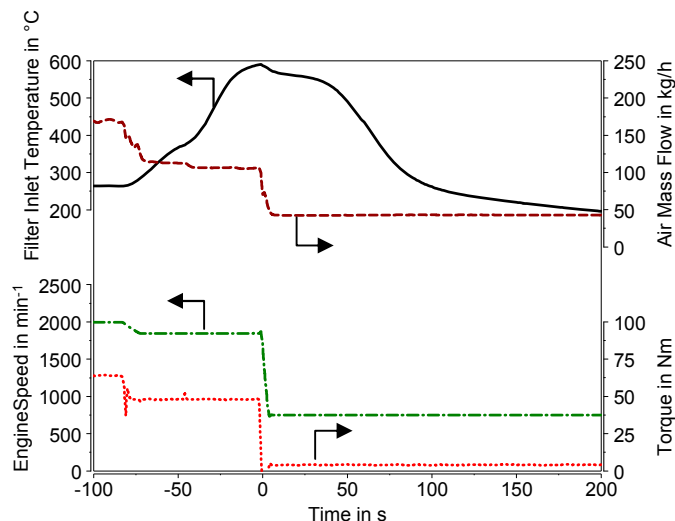


**Figure 3.** Example of a severe drop to idle (DTI) regeneration experiment. Time zero indicates when the engine is switched to idle.

## MODEL

Two types of models were used for the analysis and interpretation of the results, as well as the extrapolation to other relevant conditions

For the pressure drop calculations a 0-dimensional model was used that separates between the various pressure losses in the filter, namely inlet/outlet effects due to contraction/expansion, friction along the channels and resistance across the soot layer and the wall. The model also considers the deposition of ash as layer on the walls and as plug in the back. The model treats every

resistance separately and allows consideration for non-symmetrical channel geometries such as the asymmetric cell technology (ACT) applied to the filters used in this program [1, 2].

The simulation of the regeneration events was done by using Corning's simulator, based on a dynamic heterogeneous model of a particulate filter. The model considers for conservation of mass, enthalpy and momentum in the inlet and outlet channel as well as the channel wall. Compared to the original model described in [7] several advancements were made in the model formulation. The advanced model consists of three scales of modeling: (1) filter-scale transient heat conduction of filter volume include insulations, (2) channel scale gas flow continuity, momentum, energy balances and species transports, and (3) wall ("web") scale gas flow, species transport, and soot chemical reactions.

The filter scale heat conduction deals with the transient thermal conduction in solid (monolith filter substrate). The monolith is treated as a continuum media with anisotropic "effective" heat conduction property. The heat source accounts for heat exchange between the gas flowing in the channels and the solid walls, and also the heat generated in soot oxidation reactions and/or in any other species reactions which leads to species conversion either in soot layer or channel wall.

Channel scale model is a simplified one dimensional model for compressible gas flow with accompanying species transports. It includes viscous drag force in momentum balance of fluid flow and species mass transport perpendicular to the channel flow direction by using channel friction factor and mass transport coefficients.

Wall scale model is used for gas flow through the porous wall and associated species transport with chemical reactions. The gas flow is treated as Darcy flow with thermal equilibrium and species transport. The latter is described as purely advective (plug flow reactor model) or as advective-diffusive transport (either with a continuous stirred tank reactor model or a more accurate full advection-diffusion reactor model). The source term is derived from the kinetics of the chemical reactions occurring in the soot and the wall. For the filter scale the model is formulated for either one (axial only) or two dimensions (axial and radial). In the current study the two dimensional model was used, as the objective was to not only capture the maximum temperatures, but also the radial temperature distribution and the regeneration efficiency.

## RESULTS

### PRESSURE DROP EXPERIMENTS

The pressure drop experiments were done at clean and 8 g/dm<sup>3</sup> soot load. For the soot loading in general an accelerated method with ~5-6 g/h was used. Results are shown in Figure 4.

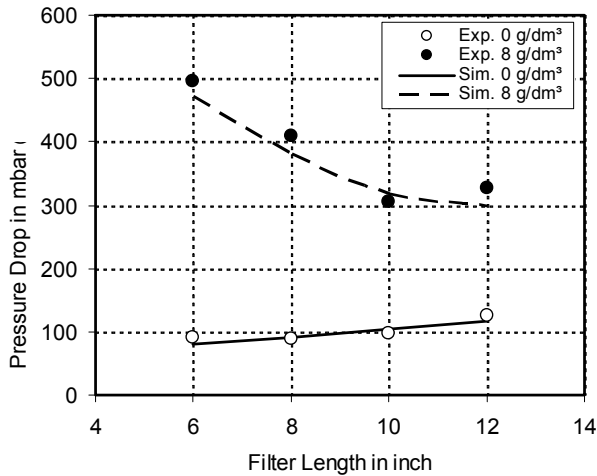


**Figure 4.** Effect of filter length on the pressure drop at 600 m<sup>3</sup>/h (note: Experimental data were at 8.0-8.4 g/dm<sup>3</sup>)

The clean pressure drop increases slightly with the filter length. This is due to the increased frictional pressure losses along the inlet and outlet channels which represent a major contribution to the overall pressure drop. The effect of a reduced pressure loss across the filter wall, due to the lower wall flow velocity with increased area, is relatively small in case of advanced filter materials with high permeability and not sufficient to balance the increased frictional losses.

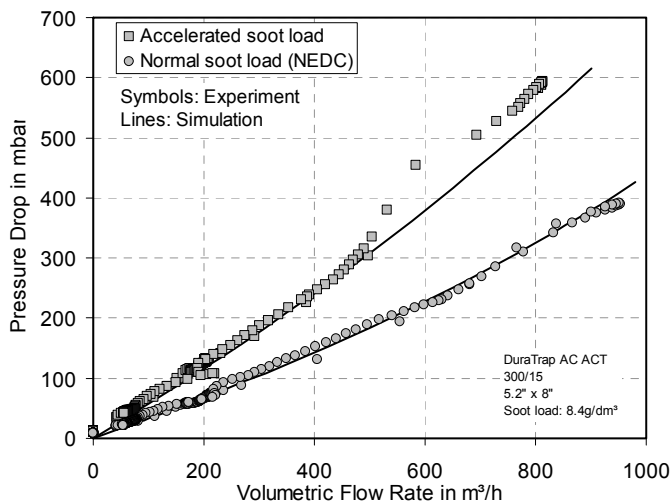


**Figure 5.** Comparison of pressure drop observed for the same filter at a soot load of 8.4 g/dm<sup>3</sup> but different soot loading procedure – accelerated vs. normal loading over simulated New European Driving Cycle (NEDC).

For the soot loaded pressure drop (~8 g/dm<sup>3</sup>) the opposite trend is observed. In this case the pressure loss across the soot layer is significant and exceeds the pressure loss due to friction. As a result, the effect of the decreasing wall flow velocity for the longer filter with higher total filtration area (and thinner soot layer) results in a lower overall pressure drop.

As mentioned earlier, the data shown in Figure 4 were obtained for soot loaded at accelerated conditions. Based

on our experience, this can lead to soot properties that are different to those of soot loaded under normal engine operation. To evaluate this effect we have also performed one experiment in which the soot was loaded over the 8" filter, but with the engine being operated over a simulated New European Driving Cycle (NEDC) with a normal calibration (EU4). This leads to a much lower soot loading rate of ~0.5-1 g/h. Results comparing the two conditions are shown in Figure 5. A significantly lower pressure drop is observed for the soot generated under the conditions with a lower soot loading rate. This would also apply to the results with filters of different length.

## REGENERATION EXPERIMENTS

The regeneration experiments were performed with all filters at comparable inlet conditions (see example shown in Fig. 3) and three different soot loads: 4 g/dm<sup>3</sup>, 6 g/dm<sup>3</sup> and 9 g/dm<sup>3</sup>.

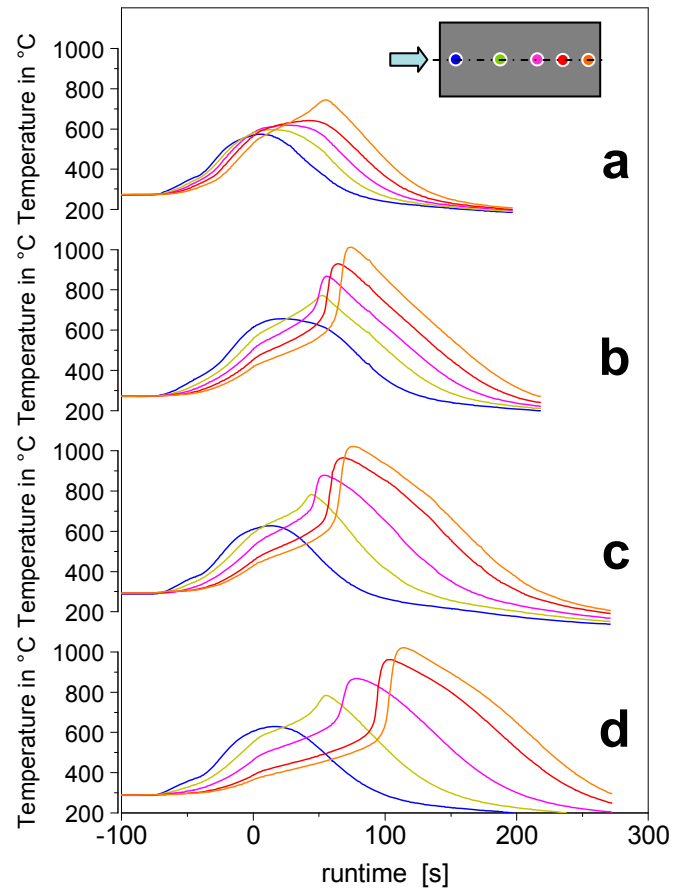


**Figure 6.** Transient temperature readings during drop to idle regeneration experiments with filters of (a) 6", (b) 8", (c) 10" and (d) 12" length. Shown are the readings at different axial positions along the center line. Initial soot load: 6 g/dm<sup>3</sup>.

### Results at Comparable Specific Soot Load

Examples of the transient temperature readings at the thermocouples located along the central axis are shown in Figure 6. The initial soot load in these cases was ~6 g/dm<sup>3</sup>. The switch back to idle occurred at the relative

time 0 s, shown in the diagram. Note, that constant specific soot mass per filter volume is used in this example. The absolute soot mass loaded in each filter prior to the regeneration was different and proportional to the filter volume.

One obvious conclusion from Figure 6 is that the highest temperatures are always observed toward the end of the filter. In addition, the maximum temperature observed increases with the length of the filter. This effect, however, is less pronounced the longer the filter gets. Comparing the short and the long filters clearly illustrates the propagation of the combustion front. For the 6" long filter, the axial temperatures increase all within a short period of time reaching the soot oxidation temperature. A significant lag can be observed for the longer filters. Here the temperature remains fairly low for a long period until the temperature also reaches about 550-600 °C, which then causes soot oxidation to initiate, coupled with the release of heat.

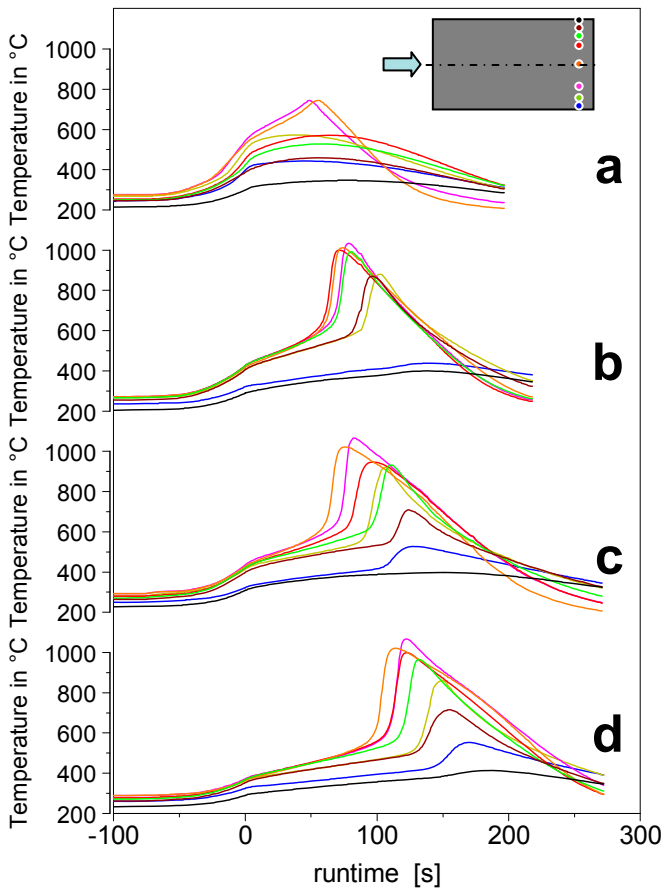


**Figure 7.** Transient temperature readings during drop to idle regeneration experiments with filters of (a) 6", (b) 8", (c) 10" and (d) 12" length. Shown are the readings at different radial positions in the last instrumented plane, 25 mm from the outlet. Initial soot load: 6 g/dm<sup>3</sup>.

In Figure 7 temperature readings at different radial positions in the last plane (25 mm from the outlet) are shown for the same experiments. From the radial temperature readings shown in Figure 7 one can see that in all cases the temperature next to the rim (last

open cell close to the filter skin) remains relatively cold for all cases. For the other temperature readings one can observe a fairly uniform temperature distribution during the heat up phase. An exception is the 6" filter experiment in which a radial temperature gradient can also be observed during this phase. For this filter setup we also had some challenges with the inlet temperature distribution due to aging of the DOC. The uniform profile observed for the filters with 8", 10" and 12" length (with only a gradient close to the filter rim) is quite typical for monolithic oxide filters, providing a good inlet distribution. For this reason it makes sense to analyze this gradient in particular as it induces thermal stress.

For the conditions of high rate of soot oxidation, the temperatures increase rapidly, and we can observe that the burning starts in the center of the filter, independent of the length. Then the combustion zone moves toward the outer area - when the temperature in these regions is sufficiently high. The heating of these areas occurs by convection but also by radial conduction. In the rim area combustion occurs last. The time span during which the combustion takes place at the different radial locations increases the longer the filter gets.

#### Effect of the Initial Soot Load

The effect of the initial soot load for the shortest (6") and the longest filters (12") is shown in Figures 8 and 9, respectively.

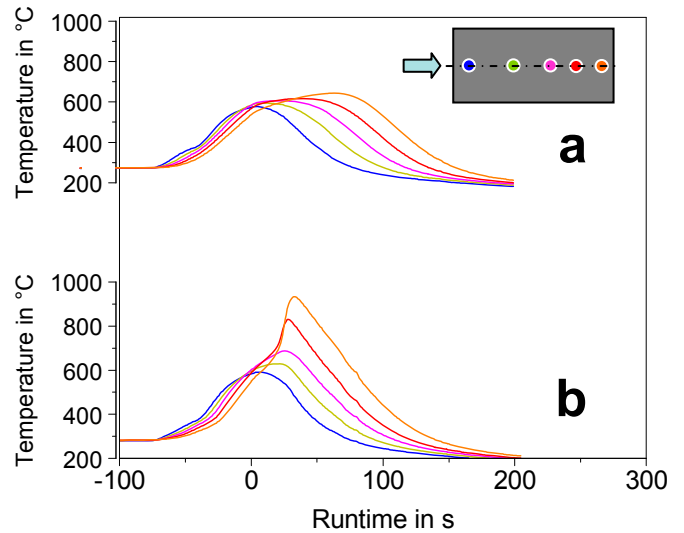


**Figure 8.** Transient temperature readings during drop to idle regeneration experiments with the 6" filter at initial soot loads of (a) 4 g/dm<sup>3</sup> and (b) 9 g/dm<sup>3</sup>. Shown are the readings at different axial positions along the center line.

For the 6" filter (Fig. 8) we can see that at 4 g/dm<sup>3</sup> soot load the soot oxidation is not sufficient to provide enough heat to keep the combustion going after the engine is switched to idle, reducing the mass flow and heat provided through the exhaust gas. On the other hand, at the higher soot load of 9 g/dm<sup>3</sup> the soot oxidation occurs within a short period of time at all axial locations ( $T$  always  $> T_{inlet}$ ).

The increase towards the end is due the accumulation of heat.

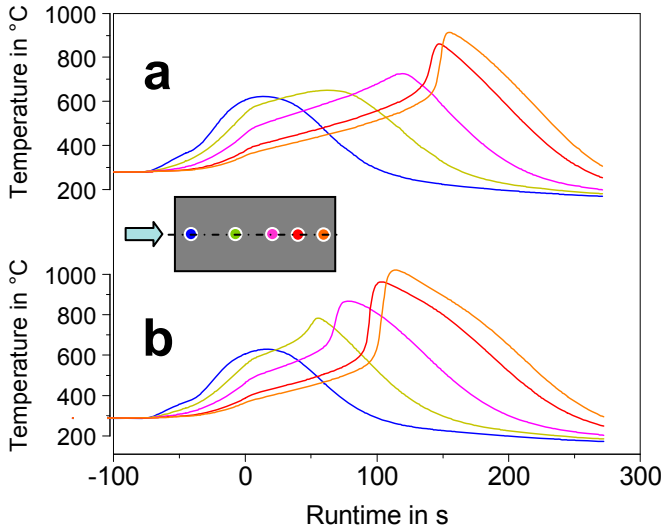


**Figure 9.** Transient temperature readings during drop to idle regeneration experiments with the 12” filter at initial soot loads of (a) 4 g/dm<sup>3</sup> and (b) 6 g/dm<sup>3</sup>. Shown are the readings at different axial positions along the center line.

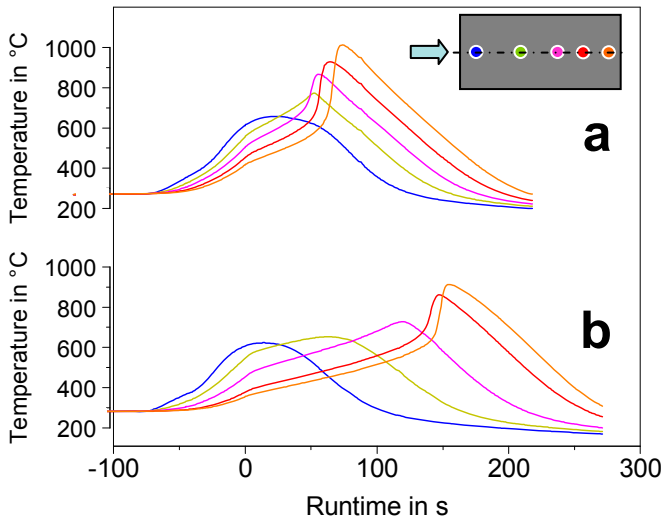


**Figure 10.** Transient temperature readings during drop to idle regeneration experiments with (a) the 8” and (b) the 12” filter at equal initial soot mass of 16.8 g. Shown are the readings at different axial positions along the center line.

For the long 12” filter (Fig. 9) different observations can be made. Here even the 4 g/dm<sup>3</sup> soot allow sustaining a certain level of soot oxidation, which eventually leads to relatively high temperatures in the rear of the filter. In the rear of the filter the heat removal is worse and the heat accumulation most expressed. The increase in soot load to 6 g/dm<sup>3</sup> leads to more heat provided from the ongoing soot oxidation, raising the level of the propagating temperature wave. The result is that the enhanced soot oxidation with the steep increase in local temperatures occurs earlier. The practical implication of this difference in behavior of filters with different length is that higher

temperatures can be expected already at lower soot loads when long filters are used.

### Comparison at Equal Absolute Initial Soot Mass

A comparison of the results obtained with the 8” and the 12” filters at an equal absolute soot mass of 16.8 g is shown in Figure 10. In this case similar maximum temperatures were observed, with actually the 8” case having a slightly higher value. In this case the effect of the length is balanced by the increased thermal mass of the longer filter at constant total energy that is released during soot oxidation.

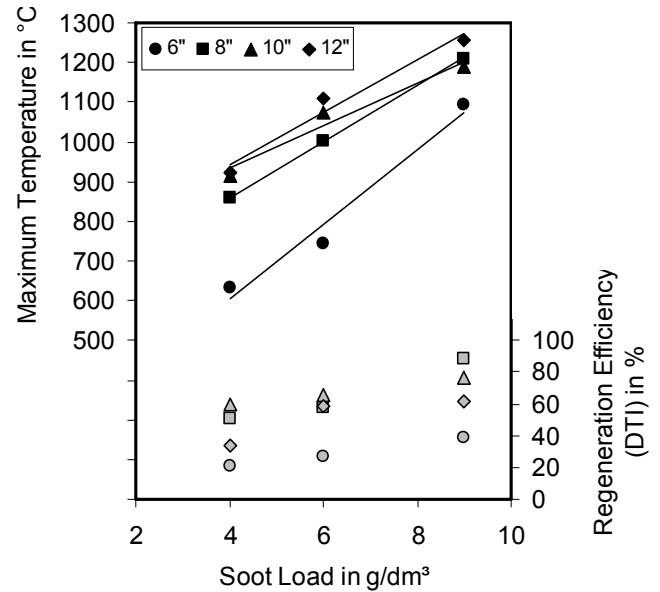


**Figure 11.** Effect of soot load on the maximum temperature and regeneration efficiency.

**Table 2.** Slope of maximum temperature vs. soot load for the filters with different length.

Filter length in inch	6”	8”	10”	12”
dT <sub>max</sub> / d(Soot Load)	93.9	70.4	53.6	65.5
in °C/(g/dm <sup>3</sup> )	Exp.	Sim.	70.3	59.6
			51.0	

In Figure 11 the maximum temperatures observed with all filters at comparable conditions are plotted vs. the initial soot load. As expected and already shown in the profiles, in all cases the maximum temperature increases with the initial soot load, following a roughly linear trend. The lowest temperatures are found for the short filter, the highest for the longest filter. Figure 11 also shows some linear trend lines, fitted to the four sets of data. Somewhat different slopes of increase in maximum temperature vs. soot load can be identified, with the values provided in Table 2. All values and their average of 71 °C/(g/dm<sup>3</sup>), however, represent the typical range observed commonly with oxide filter materials.

It should be mentioned that the maximum temperatures observed for these filters with 8”-12” length at 9 g/dm<sup>3</sup>

soot load are outside of what would be recommended for cordierite filters. The results show that adapted regeneration strategies are required to allow for the application of cordierite filters at high soot loads.

In addition to the peak temperatures, the regeneration efficiency observed in these interrupted DTI regenerations is provided in Figure 11. Here, the lowest values by far are found for the short 6" long filter. For the other three filters comparable regeneration efficiencies were observed, mostly in the range of 50-80 percent. Although a detailed discussion will be provided later, one can already suspect that there is a correlation between the temperatures observed and the regeneration efficiency. Considering the temperature readings shown earlier, one can see that for the short filter the combustion stops fairly shortly after the engine is brought back to idle; no progression of the combustion front is visible. For the longer filters the soot oxidation is not quenched, but as already mentioned earlier, a combustion front propagates through the filter, enabling higher regeneration efficiency and higher temperatures.

The effect of the soot mass burned becomes even clearer in Figure 12 in which the maximum temperature is plotted as a function of the soot mass burned. All data fall into a single correlation, independent of the length. What is interesting to note is that the relationship observed is not linear. After an initial (linear) increase, the maximum temperature seems to level off to a constant peak temperature. This observation will be discussed in more detail in the next section.

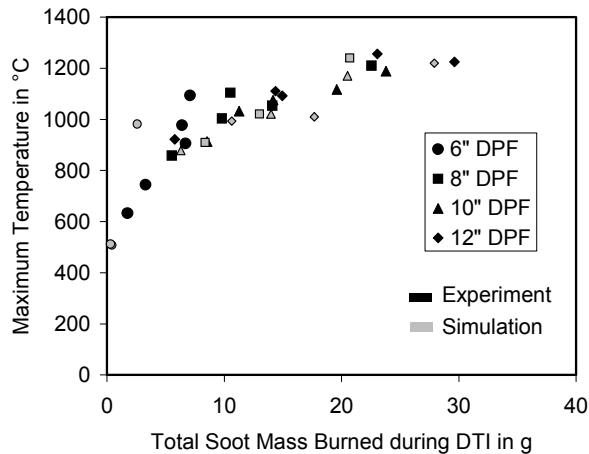


**Figure 12.** Maximum regeneration temperature vs. total soot mass burned. Black symbols show experimental and grey symbols simulated data.

#### Analysis of Radial and Axial Gradients

Besides the maximum temperatures, it is also of interest to compare the observed maximum gradients. The thermocouple pattern shown in Figure 2 allows measuring the radial gradient in the region close to the skin with a very good resolution. There are several pairs of thermocouples with a spacing of 10 mm with one

thermocouple placed directly into the last open channel before the skin. In Figure 13 the transient of the maximum radial gradient measured at any of the thermocouple pairs is shown for the examples already described in Figure 6. The different peaks are due to the spatial separation of the different thermocouple pairs. For example, each peak represents the time when the thermal wave passes one of the thermocouple pairs. The basis of the gradient can also be understood by Figure 7 as well. The largest gradient usually occurs when the temperature inside the filter reaches its peak while the combustion in the rim area has not yet started (or does not start at all.)

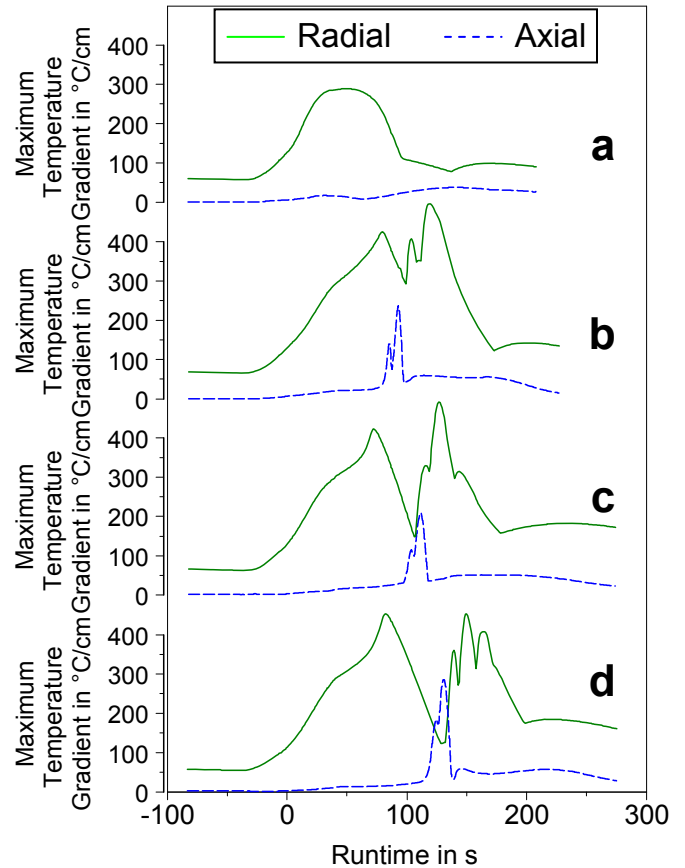


**Figure 13.** Transients of the recorded maximum radial and axial gradients for the regenerations shown in Figure 6. Filter length: (a) 6", (b) 8", (c) 10" and (d) 12".

Usually a good correlation for oxide filters is observed between the maximum temperature inside the filter and the maximum radial gradient measured with these pairs of thermocouples. A plot of the measured maximum radial temperature gradients vs. the maximum temperatures is given in Figure 14. One can see that although the absolute values of the shorter filters are lower (as shown before), the data for all filters fall into a single correlation. The results therefore suggest that the length does not affect the maximum radial gradient. It is rather the maximum temperature that drives this value, in addition to other factors such as inlet temperature, flow distribution, and radial heat losses through the mat and can. One should also note that the high gradients observed in some of the experiments would lead to the

formation of some level of radial cracks with any cordierite filter.

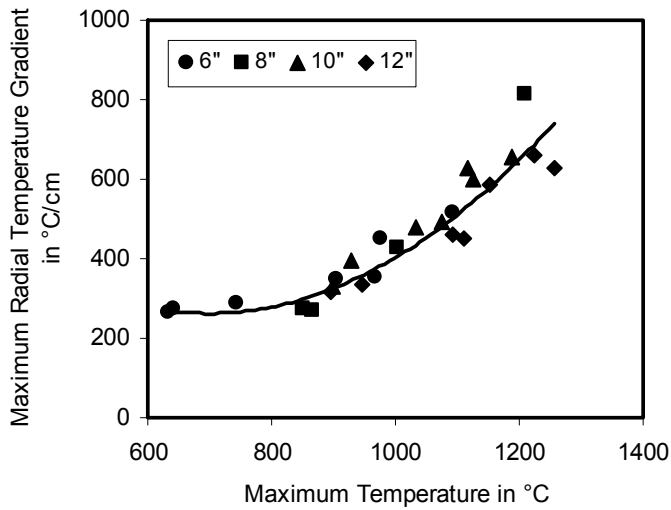


**Figure 14.** Correlation between the maximum radial temperature gradient and the maximum temperature. Note: the maximum gradient is measured with one of the thermocouples pairs located close to the skin and with 10 mm spacing.

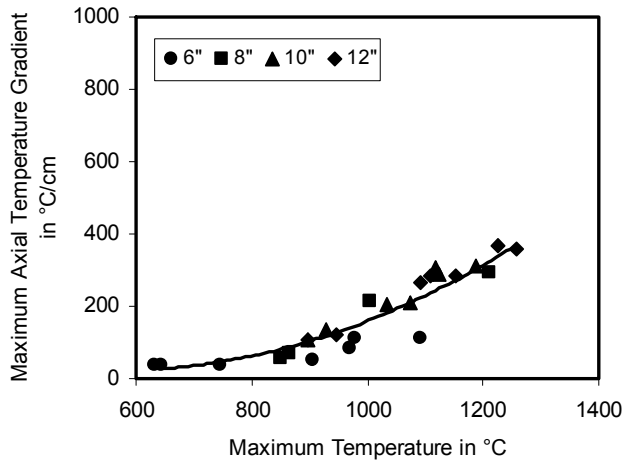


**Figure 15.** Correlation between the maximum axial temperature gradient and the maximum temperature. Note: the maximum gradient is measured with one of the thermocouples pairs with 10 mm spacing

The thermocouple installation also allowed measurement of the maximum axial gradient in the rear of the filter with a high resolution of 10 mm (see Fig. 2). In Figure 13 the transient of the maximum axial gradients are shown for the examples of Figure 6. One obvious observation is that the level of the axial gradients is generally lower than for the radial gradients. Also, they only occur for the short period during which the combustion front passes through each location. In Figure 15 the measured axial gradients are summarized and plotted vs. the maximum filter temperature for the filters with different lengths. Again, the comparison with Figure 14 shows the lower

level of the measured maximum axial gradients compared to the radial gradients.

## COMPARISON WITH MODEL PREDICTIONS

As we want to use the model for the analysis of the observations, first a comparison between the simulation and the experiments will be provided. In Figure 16 the calculated temperature readings along the centerline are shown for the 8" and 12" filters at equal initial soot mass of 16.8 g. The corresponding experimental data were shown earlier in Figure 10. Generally, good agreement can be observed.

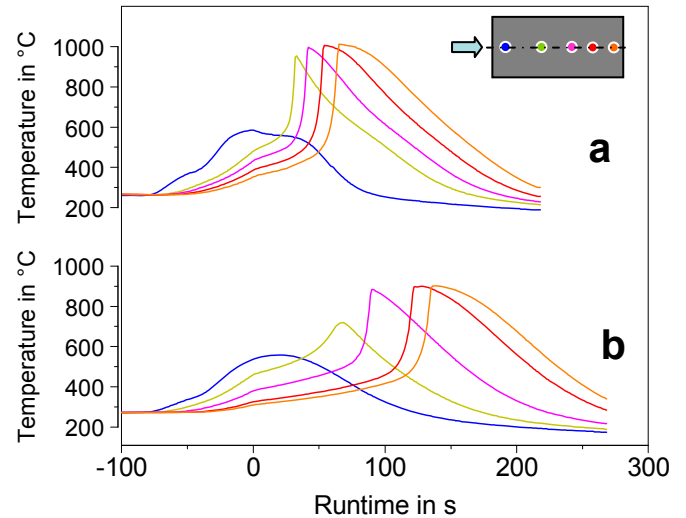


**Figure 16.** Simulated transient temperature profiles during drop to idle regeneration experiments with the (a) 8" and the (b) 12" filter at initial soot loads of 16.8 g total. Shown are the data at different axial positions along the center line.

As mentioned earlier, a key variable is the maximum temperature of the filter. Table 3 provides a direct comparison of the peak temperatures measured on and predicted for the 8" filter at different soot loads. Table 3 also provides a comparison of the regeneration efficiencies measured and predicted. For both values good agreement is observed. It should be mentioned that the use of a one dimensional regeneration model is capable of capturing the maximum temperatures but the regeneration efficiencies predicted would be much higher. This discrepancy is caused by residual soot in the rim area where lower temperatures are observed. The comparison in Table 4 shows that the model can also capture the length effect with respect to both the peak temperatures and regeneration efficiency. The fact is that the maximum temperature for the 10" filter is slightly lower due to some small differences in the actual experimental conditions. Although the soot loading was done with a relatively tight tolerance of  $\pm 0.5\text{g/dm}^3$  the actual soot load in the experiments deviated slightly from the target values. Similar is true for the temperature which varied, mainly due to deactivation of the DOC throughout the test program. In the simulation this is

considered by using the appropriate boundary and initial conditions. Therefore, the simulated results show the same variations.

**Table 3.** Comparison of simulation and experiment at for DTI regenerations with the 8" filter at different initial soot load.

Soot Load		4 g/dm <sup>3</sup>	6 g/dm <sup>3</sup>	9 g/dm <sup>3</sup>
$T_{max}$	Experiment	858 °C	1003 °C	1210 °C
	Simulation	909 °C	1020 °C	1240 °C
$\eta_{Reg}$	Experiment	51 %	58 %	88 %
	Simulation	67 %	82 %	82 %

**Table 4.** Comparison of simulation and experiment at for the filters with different length at equal initial soot load of 9 g/dm<sup>3</sup>.

Filter Length		6"	8"	10"	12"
$T_{max}$	Experiment	1093 °C	1210 °C	1188 °C	1256 °C
	Simulation	981 °C	1240 °C	1170 °C	1220 °C
$\eta_{Reg}$	Experiment	39 %	88 %	76 %	62 %
	Simulation	14 %	82 %	66 %	76 %

More comparison has already been shown in Figure 12 where one can find the same correlation between the soot burned and the maximum temperature for both experiment and simulation.

Furthermore, Table 2 shows that we find the same slope of the increase in peak temperature vs. soot load as from the experiments.

In summary, a reasonable agreement between the predictions of 2D model and the experimental observations is found, covering the range of variables considered in the study.

## DISCUSSION

To understand the impact of the filter length, one approach is to look at the spatial distribution of the soot and the temperature within the filter at different time steps. This is shown in Figures 17 and 18 for the 8" and 12" long filter, respectively, at an initial soot load of 6 g/dm<sup>3</sup>. Since these spatial distributions are not experimentally available, we have to rely on the modeling tools.

From the profiles in Figures 17 and 18 we can clearly see the process of soot combustion during these DTI experiments. Initially, the soot starts burning in the front of the filter only (regime marked with an "a"). After the engine is switched back to idle the inlet temperature decreases. As a result, the soot burning in the very front stops and some soot remains. Inside the filter then the combustion front develops (profiles marked with a "b") and propagates at a relatively constant speed (suggesting a constant burning rate) towards the filter

outlet. The analogous observations are made by looking at the temperature profiles. For both examples (Figures 17 and 18) the profiles are shown at identical time steps, e.g. at the beginning and from 140 s on in 10 s intervals. Comparing the profiles for the 8" and the 12" filter shows that in case of the shorter filter (8") the burning at the inlet part is significantly more effective than for the long filter (12"). Less soot remains and the length with residual soot is shorter.

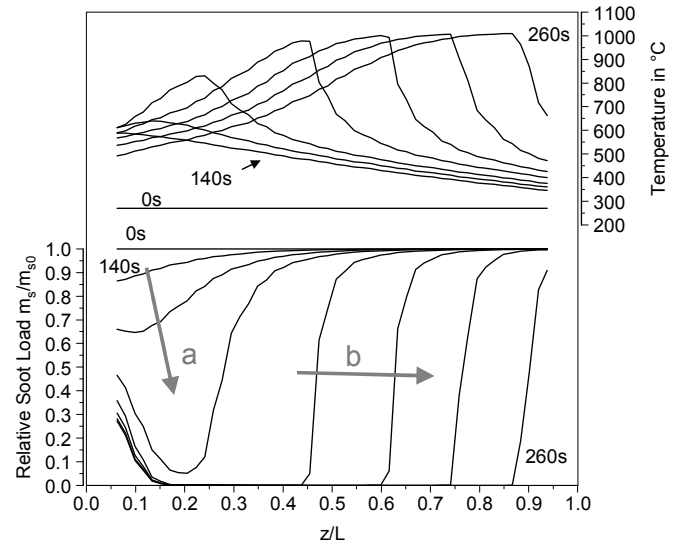


**Figure 17.** Spatial soot (bottom) and temperature (top) profiles inside the filter at different time steps (0 s, 140 s to 200 s in 10 s intervals). Simulation results for the L=8" filter at 6 g/dm<sup>3</sup>.  $m_s$ : actual soot load,  $m_{s0}$ : initial soot load,  $z/L$ : dimensionless length.

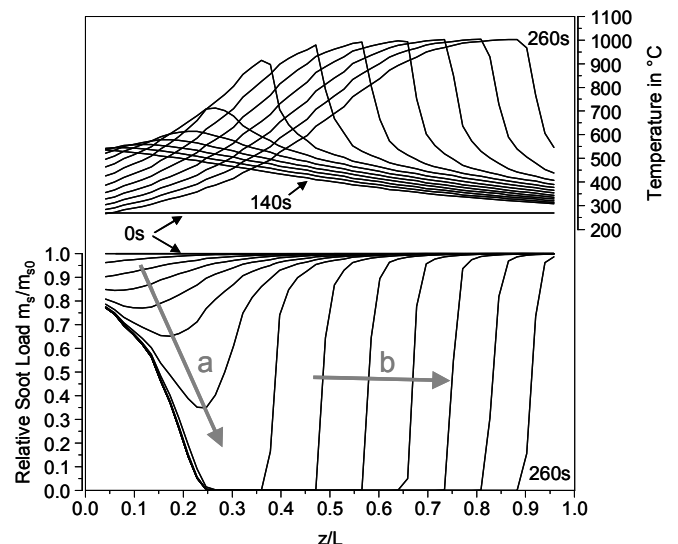


**Figure 18.** Spatial soot (bottom) and temperature (top) profiles inside the filter at different time steps (0 s, 140 s to 260 s in 10 s intervals). Simulation results for the L=12" filter at 6 g/dm<sup>3</sup>.  $m_s$ : actual soot load,  $m_{s0}$ : initial soot load,  $z/L$ : dimensionless length.

The profile of the combustion front looks very similar in both cases and we can immediately recognize that the reaction front is propagating at a higher velocity ahead of

the thermal wave. The thermal wave is characterized by the smooth increase in the temperature profiles downstream of the maximum temperature value of each curve. The profiles are actually showing the cooling by the colder inlet gas. The propagation of the thermal wave occurs at a velocity of roughly  $u_T=1.27-1.28$  mm/s, in line with the theoretical value [10] obtained from

$$u_T = \frac{\dot{m} \cdot c_{pG}}{A_{CPF} \cdot c_s \cdot \rho_{CPF}}$$

with  $\dot{m}$  as mass flow,  $c_{pG}$  and  $c_s$  as heat capacity of the gas and solid, respectively,  $A_{CPF}$  as frontal area and  $\rho_{CPF}$  as bulk density of the filter.

The propagation of the reaction front can be clearly seen by the soot profiles and the steep decline in the temperature profiles (right part of the temperature profiles). Downstream the temperature is still low as the reaction has not yet reached this area. Upstream, reaction has taken place. The propagation velocity of the combustion front is roughly 2.9 mm/s. This is also in perfect agreement with the theoretical value for the propagation velocity [10], for which we have to use the information about the oxygen consumption  $\Delta w_{O_2}$  between inlet and outlet

$$u_R = \frac{\dot{m} \cdot \Delta w_{O_2}}{A_{CPF} \cdot (m_s / V_{CPF})}$$

with  $m_s$  and  $V_{CPF}$  as soot mass and filter volume, respectively. The propagation at constant rate can also be seen from the transient oxygen concentration measured at the filter outlet. In Figure 19 this is shown for experiments with all filters at an initial soot load of  $\sim 8$  g/dm<sup>3</sup>. The area between the inlet oxygen concentration and the outlet concentration is proportional to the amount of carbon burned (e.g. the time integral of mass flow times the difference between the inlet and outlet oxygen concentration, assuming full conversion of any gas phase HC or CO by the upstream DOC).

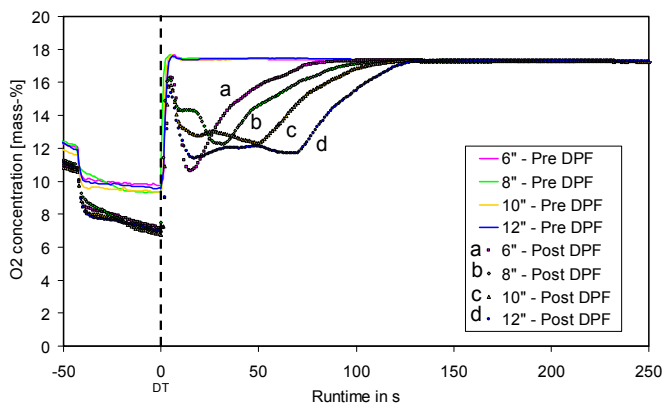


**Figure 19.** Experimental oxygen concentration up and downstream of the filters with different length during a drop to idle experiment at equal specific soot load of 8 g/dm<sup>3</sup>.

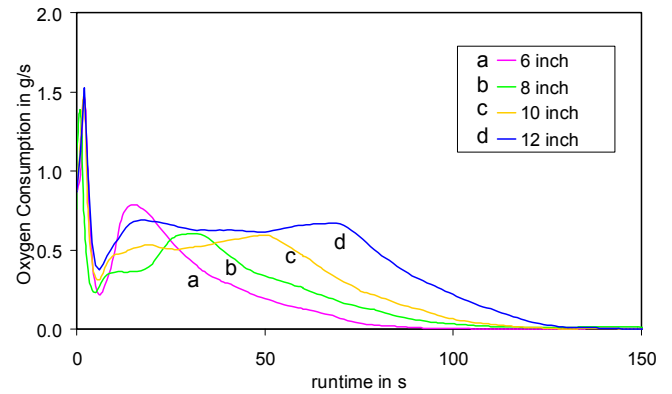


**Figure 20.** Oxygen consumption rate during the DTI experiments shown in Figure 19. Initial soot load 8 g/dm<sup>3</sup>.

This rate of oxygen consumption is shown in Figure 20. After a rapid initial increase in consumption and decrease in the oxygen concentration during the first seconds, the rate of consumption and the outlet oxygen concentration remains relatively constant until the soot combustion ends. Then the oxygen consumption decreases to zero and the outlet concentration equals the inlet. Integrating the oxygen consumption rate and comparing it to the related mass of carbon burned yields a good agreement. When comparing the results for the filters with different lengths we observe that the initial peak in oxygen consumption is comparable for all filters. The plateau values in oxygen consumption and outlet concentration are also similar, although a slight increasing trend can be seen when going from 8" to 12". For the short filter, however, no real plateau is formed but the consumption instead goes through a short peak with the maximum rate being the highest for any filter length. In this case the combustion takes place in a large portion of the filter throughout the entire regeneration process; a combustion front propagating through the filter is not formed.

The impact of the soot load on the oxygen consumption is shown in Figure 21. Results shown are from the simulation. The qualitative profiles with a short initial peak followed by the plateau are also observed in the simulation, showing again good agreement with the experiment. Comparing the results at different soot loads delivers the expected increase in consumption, e.g. low oxygen outlet concentration when the soot load is higher. Also influenced by the soot load is the significance of the initial peak in consumption, as well as the duration during which oxygen is consumed (or soot is burned). The differences in the duration of the oxidation phase can be well understood considering the results discussed above. The increase in soot load results in an increase in the temperature level and a more than proportional increase in the oxygen consumption  $\Delta w_{O_2}$ . The combined effect is acceleration in the velocity at which the reaction front propagates.

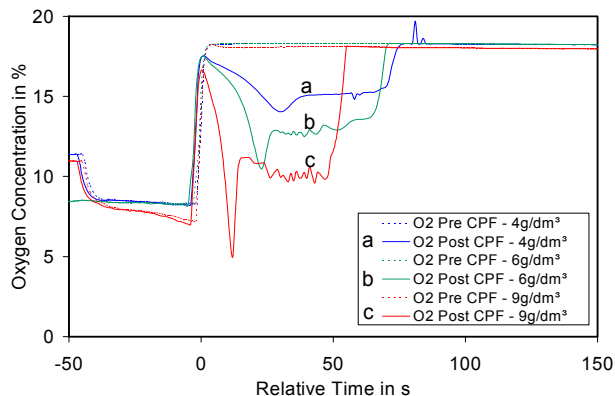


**Figure 21.** Simulated oxygen concentration up and downstream of the 8" filter during DTI experiments with different initial soot load.

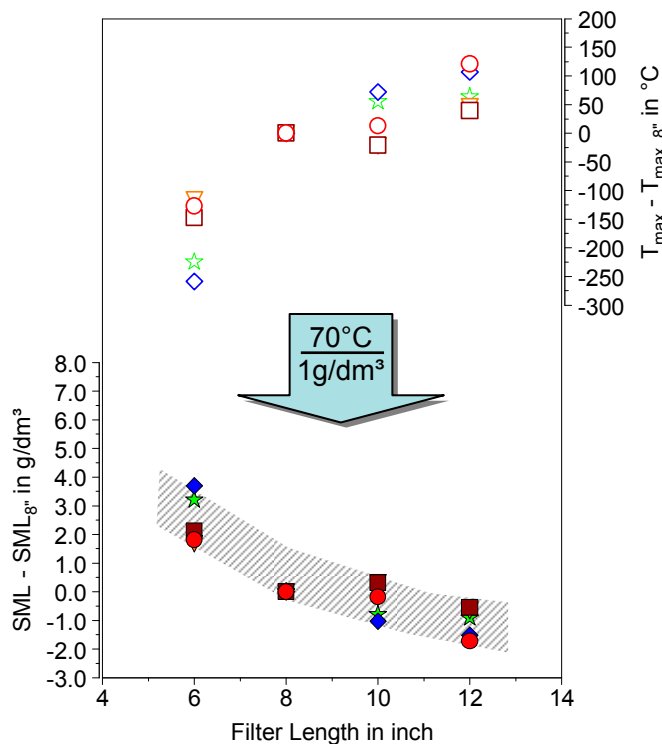


**Figure 22.** Impact of filter length on the maximum temperature relative to a filter with 8" length (top) and conversion to a relative soot mass limit relationship based on the experimental data and an assumed  $d(T_{max})/d(\text{Soot Load}) \approx 70 \text{ }^\circ\text{C}/(\text{g}_{\text{soot}}/\text{dm}^3)$ . Symbols represent data from experiments with different calibration and soot load.

For the practical application the effect of the filter length on the maximum soot capacity of a filter is important information. Usually, the maximum soot capacity of a filter is determined by the maximum temperature that occurs during worst case conditions, such as the drop to idle experiments discussed in this paper. For a given material this maximum temperature could be assumed to be independent of the filter length or size. One way to estimate the impact of the filter length on the soot capacity is to extract the maximum temperatures

observed with the filters of different lengths and compare them at equal specific soot loads. This is shown in the top part of Figure 22. The differences in peak temperatures observed are normalized with the values found with the 8" filter, which is used as reference. To convert this into the effect on the soot mass limit of a filter, we can make use of the correlation between the increase in peak temperature and soot load, which we have described earlier (see Figure 11 and Table 2). An average gradient of  $\sim 70 \text{ }^\circ\text{C}$  per  $\text{g}/\text{dm}^3$  in soot load was found (in both the experiments and the simulations). If we now divide the relative peak temperatures shown in Figure 22 (top) by this average gradient, we can obtain an estimate of the impact the length has on the soot mass limit, shown in the bottom of Figure 22. As we have used the 8" as reference the data are relative to this filter length.

Due to the scatter in the experimental data the correlation is a band, not a narrow line. Nevertheless, the data shown in Figure 22 can help to estimate the impact the filter length can have on the soot mass limit. One conclusion is that increasing the filter length for example from 6" to 12" does not double the absolute soot mass capacity of the filter (in grams). Instead there is some penalty due to the lower specific soot capacity (in  $\text{g}/\text{dm}^3$ ) of the longer filter. Although derived for cordierite filters, the results shown in Figure 22 are expected to be also useful to make estimates for other oxide filters with low thermal conductivity as the physics are similar.

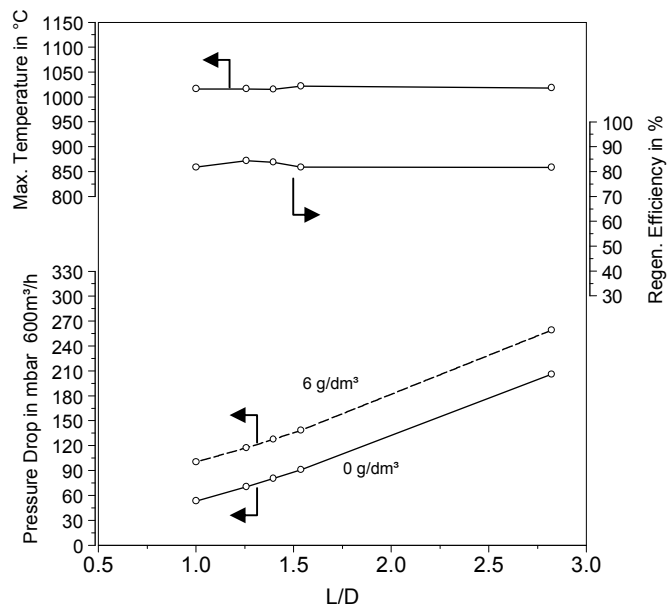


**Figure 23.** Impact of the length to diameter ratio,  $L/D$ , for filters with constant volume of  $2.78 \text{ dm}^3$ . Maximum temperature and regeneration efficiency for DTI regenerations at  $6 \text{ g}/\text{dm}^3$  initial soot load. Pressure drop at  $600 \text{ m}^3/\text{h}$ .

So far we have only evaluated the influence of the filter length at equal diameter or frontal area. Another relevant option is the design for different length to diameter ratios for filters with equal volume. Simulated results for a

constant filter volume of 2.78 dm<sup>3</sup> are shown in Figure 23.

For the maximum temperature during DTI no major differences are observed under the used conditions. The regeneration efficiency is also relatively constant. The strongest impact of the L/D ratio is on the pressure drop. Results are shown for the clean and soot loaded (6 g/dm<sup>3</sup>) filter at 600 m<sup>3</sup>/h. Due to the increase in frictional pressure losses, which scale linearly with the length, a roughly linear increase in pressure drop with increase in length to diameter ratio (L/D) is observed. This demonstrates that for practical applications filters with low L/D ratio are favorable.

## CONCLUSION

The effect of the filter length on the pressure drop and regeneration behavior of oxide diesel particulate filters has been discussed in detail by means of experimental data and detailed numerical simulations. The clean filter pressure drop increases with the filter length. The limiting factor is the friction along the channels. For the soot loaded state the opposite trend is observed: the lower wall flow velocity dominates, leading to lower losses across the soot layer.

For the worst case regeneration experiments, generally equal or lower temperatures were observed with shorter filters. This is partially related to the amount of soot available for combustion, as we have found a good correlation between the soot mass burned and the maximum temperature. For the experiments performed, a significant length effect has been found between 6" and 8", whereas the differences between 8" and 12" were less significant. The length effect has been combined with the observed correlation between initial soot load and peak temperature (Fig. 22) to allow for a rough estimate of the influence the filter length has on the soot mass limit of the filter.

The maximum filter temperature has been found to correlate well to the maximum radial and axial gradient inside the filter. This value can therefore be used for guidance if limited temperature information is available.

The simulation tool has been used to analyze the experimental findings and to illustrate the phenomena occurring during the worst case regenerations. It was shown that the overall process is determined by the differences in the propagation of the combustion front and the thermal wave. For the range of conditions studied, the latter was always slower. For the longer filters, stable conditions were reached with constant front propagation and constant oxygen consumption / soot burning rate.

With respect to the length to diameter ratio, L/D, low values have been found to provide the best results, especially with respect to pressure drop.

The data and results reported in this paper are based on tests conducted using certain apparatus and conditions with specific vehicles, systems, components, coatings, catalysts, and /or controls. Results in other applications may differ based on conditions, apparatus, and other factors, including but not limited to the vehicles, systems, components, coatings, catalysts, and controls used.

## ACKNOWLEDGMENTS

The authors want to thank Thomas Bürgermeister and Marco Burkard from ElringKlinger Motortechnik GmbH for the excellent execution of the experiments, Maxim Sokolov and Leslie Button from Corning Incorporated for their contribution to the development of advanced regeneration model.

## REFERENCES

1. Kercher L., Rose D., Boger T., W.A. Cutler, R. Dorenkamp and T. Duesterdiek. "Application of a New Filter Material in Volkswagen's Diesel Particulate Filter Systems". 3<sup>rd</sup> Emission Control Conference, Dresden 2006.
2. Rose D., O.A: Pittner, C. Jaskula, T. Boger, T. Glasson and V. Miranda DaCosta. "On Road Durability and Field Experience Obtained with an Aluminum Titanate Diesel Particulate Filter". SAE 2007-01-1269
3. Cutler W.A., T. Boger, A.F: Chiffey, P.R. Phillips, D. Swallow and M.V. Twigg. "Performance Aspects of New Catalyzed Diesel Soot Filters Based on Advanced Oxide Filter Materials". SAE 2007-01-1268
4. Adelman B., Karkkainen A., P. Berke, A. Heibel, T. Parker and D. Pickles. "Development and Application of a US-EPA '07 Particulate Filter System for a 7.6l I-6 Medium Duty Truck Engine. 15<sup>th</sup> Aachen Kolloquium Fahrzeug- und Motorentechnik, Aachen 2006.
5. Heibel A. and U. Zink. "Lösungen zur Einhaltung der Grenzwerte für Nutzfahrzeugemissionen der nächsten Dekade basierend auf EPA 2007 und EU V" (*engl.* „Technical Paths to Emission Regulation Compliance of Commercial Vehicles in the NExt Decade based upon Solutions for EPA 2007 and EUV"). MTZ (68) 07-08/2007, p. 570-574
6. Boger T., D. Rose, I.-C. Tilgner and A.K. Heibel. "Regeneration Strategies for an Enhanced Thermal Management of Oxide Diesel Particulate Filters", paper submitted to SAE 08PFL-510
7. Bhatia G. and N. Gunasekaran, "Heat-Up of Diesel Particulate Filters: 2D Continuum Modeling and Experimental Results", SAE 2003-01-0837

8. Mizutani T., M. Ito, N. Masukawa, S. Ichikawa, K. Yuuki, H. Kurachi, T. Toyoshima, T. Ito, I. Lappas, A. Schaefer-Sindlinger and C.-D. Vogt. "The Study for Structural Design of the Segmented SiC-DPF", SAE 2006-01-1527
9. Ohno, K., K. Shimato, N. Taoka, H. Santae, T. Ninomiya, T. Komori and O. Salvat. "Characterization of SiC-DPF for passenger car", SAE 2000-01-0185
10. Salden A. „Adsorption / Incineration Processes for Waste Gas Purification“. PhD Thesis, University of Stuttgart (2001)